Real Single Grain Grinding Finite Element Method Simulation for Case-Hardened Steel Based on Equivalent Contact Area Analysis

Real Single Grain Grinding Finite Element Method Simulation for Case-Hardened Steel Based on Equivalent Contact Area Analysis

Flavia Lerra[1] Erica Liverani Enrico Landi Alessandro Fortunato

Grinding is an indispensable phase in the gear production chain as it allows very stringent requirements characteristic of the automotive sector to be satisfied. The main goal of this finishing process is to ensure compliance with the surface integrity and dimensional toler-ance specifications of the product. A single-grain grinding FEM model has been implemented to predict grinding load values based on real grain geometry using a set of Johnson & Cook coefficients able to represent the flow stress curve of a typical gear case-hardened steel 27MnCr5. Grain geometry acquired through computed tomography was imported into three-dimensional process simulation software DEFORM-3D. As the use of real grain geometry leads to time-consuming simulations, an equivalent defined geometry grain was implemented to compare the cutting behavior and calculate maximum force values through real contact area analysis under the same process param-eters. Calculated loads were subsequently compared with experimental results, showing good agreement with a maximum percentage difference less than 13% for two different grain geometries. Grinding force measurements were performed in a single-grain configu-ration on a CNC surface grinding machine adopting a wheel speed of 384 rad/s, a feed rate of 8.6 mm/s and a depth of cut of 0.1 mm. [DOI: 10.1115/1.4051536]

Keywords: dry grinding, case-hardened steel, single-grit FEM simulation, gears, advanced materials and processing, grinding and abrasive processes, micro- and nano-machining and processing, modeling and simulation, FEM modeling

Introduction

Grinding is a fundamental stage of automotive gear production where stringent quality requirements must be satisfied. Nowadays, automotive gears are characterized by a series of technical specifications that make them one of the most complex products to produce. Recently, dry grinding has been verified as a suitable gear finishing technology that not only allows specific technical requirements to be satisfied but leads to a cleaner production chain with a substantial reduction in costs and a healthier workplace [1]. The absence of lubricant can potentially lead to thermal burns and rejection of products, for which it is mandatory to optimize the finishing grinding phase accurately. Therefore, the grinding process must be correctly implemented and optimized [2].

Many models have been developed to analyze and optimize the grinding process with the scope of forecasting results in terms of surface finish and microstructural integrity [3]. Such models are generally divided into those whose outputs can be verified on the macroscale and those whose results apply to the microscale [4]. In the first case, the interaction between the whole grinding wheel and the workpiece is analyzed and thermal aspects are mainly considered. In the second, the interaction between a single grinding grain and the part is analyzed by studying the different engagement mechanisms. Analytical and numerical macro-scale models forecast thermal responses in grinding, replacing the action of the grinding wheel with a moving heat source. The heat source is generally defined as a heat flux generated by the removal mechanism, calculated as:

$$q_w = \frac{\varepsilon P}{l_c b}$$

where l_c and b are the contact arc length and width, P is the grinding power and ϵ the energy partition ratio. The grinding power represents the main contribution in calculating the heat flux and is usually measured experimentally, while greater difficulties are found in obtaining the real value of the energy partition ratio. This parameter represents the proportion of heat absorbed by the workpiece and, together with the heat flux distribution, has been the focus of many studies dealing with grinding thermal models [5–9].

Micro-scale models tend to consider the physics behind grinding, with several different approaches having been presented over time. Many analytical models have been developed to forecast loads during the grinding process. Tonshoff et al. compared different approaches to modeling the resulting topography, chip formation, forces and surface integrity [10]. Rowe et al. presented an extensive study, divided into four parts, relating to the analytical simulation of abrasive wheel dressing and grinding forces correlated with experimental data and wheel wear analyses [11–14]. Warnecke's geometric and kinematic models aimed to generate a wheel prototype with an optimized defined grain structure to forecast grinding forces and surface quality by considering the average geometric engagement between a virtual wheel and the workpiece [15,16]. Other authors considered the average undeformed chip thickness as a function of material properties, kinematic conditions and dynamic effects assuming a Rayleigh probability density [17]. Wang et al. instead proposed an analytical model to quantify rubbing, ploughing and cutting forces in the time domain [18]. Each of these models, although accurate, is based on prior knowledge of many constants. Experiments are therefore usually required to determine the value of coefficients for a specific set of parameters, while in many cases the models do not consider material behavior.

Numerical FEM simulations usually take on a different approach, considering the material flow stress but requiring huge calculation power. The micro-scale problem has been studied with both 2D simulations to reduce data generation [19] and 3D simulations

[1]Corresponding author.

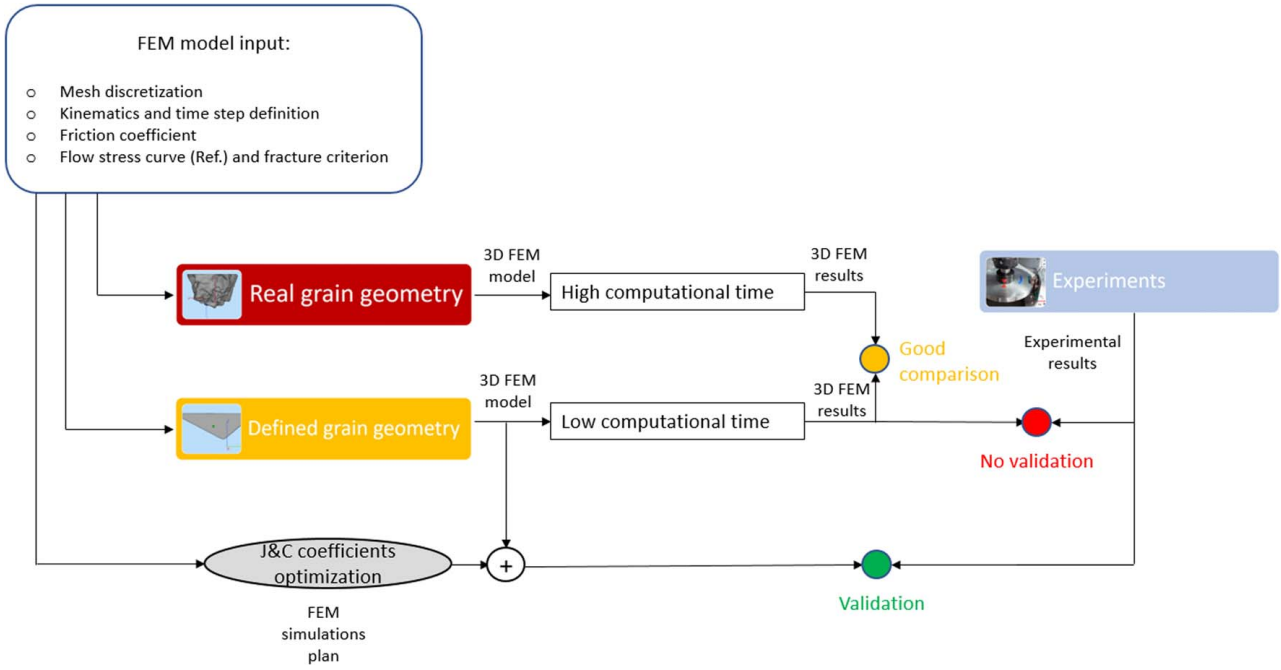

Fig. 1 Flow diagram of modeling approach and experimental verification

that introduce a randomly defined grain shape represented by a pyramidal asperity [20]. However, a more detailed model is required to correctly represent phenomena taking place during the grinding process. Bauer et al. developed a 3D model by representing the abrasive grain as a sphere and modeling the workpiece based on the combination of multi-material Eulerian and Lagrangian elements [21]. They demonstrated a reduction in the material pile-up with increasing cutting speed, together with a rise in normal forces due to material hardening and a reduction in tangential forces due to lower friction between the tool and workpiece. Single-grit FEM simulations were also carried out by Zhu, who provided validation by matching forces and temperatures with experimental data [22]. Öpöz et al. developed a 3D model and considered material pile-up area and forces over three consecutive passes [23].

Within this context, the present paper proposes a micro-scale approach using a 3D single-grit model to predict forces during grain-workpiece interaction in dry conditions implementing a new flow stress curve for the case-hardened depth of typical steel employed for automotive gears (27MnCr5). An initial simulation was implemented based on the real grain geometry, after which an equivalent defined grain geometry was designed to facilitate computational aspects. The equivalent defined grain geometry was obtained by considering the rake angle, tip radius, opening angle and width of the real grain, taking care to conserve the same grain orientation during experiments. Correspondence between the behavior of the simplified equivalent grain and the real geometry was first verified in terms of load values using the Johnson & Cook (J&C) coefficients of reference material. Subsequently, starting from the reference material an inverse parameter identification was performed to optimize the flow stress curve for the steel in question by replacing previous material coefficients with more accurate values, better representing the behavior of the measured hardness of the case-hardened 27MnCr5 steel. A simulation plan was developed to check and calibrate the Johnson & Cook constitutive material coefficients. The model also considered the real kinematics of the grinding process, which implies multiple rotations of the same abrasive grain on the workpiece surface. Model validation was performed by comparing tangential and normal loads with experimental data for two different grain geometries belonging to the same abrasive class material and size. The good agreement between the models confirmed that the simulation with a simplified abrasive grain is a viable way to model the grinding process and the flow stress coefficient adopted is suitable to describe the behavior of the case-hardened depth of a typical automotive gear steel under cutting conditions.

Single Grain Grinding Model

The modeling approach employed within this work, shown schematically in Fig. 1, is based on three simulation approaches using the same FEM input parameters such as mesh discretization, kinematics, time step, friction coefficient and fracture criterion. The first approach adopts the real grain geometry acquired through computed tomography and the flow stress curve coefficients of reference material. The second sees the replacement of the real grain with an equivalent defined grain geometry using the same material flow stress curve. Finally, the third simulation approach adopts the same equivalent defined grain but employs a new optimized material flow stress curve. Calibration of the flow stress curve was performed by means of a simulations plan based on the maximum cutting depth reached during the process varying J&C coefficients. The outcomes of each simulation approach were analyzed in detail and compared with experimental results.

FEM Model. A thermomechanical FEM simulation was implemented in DEFORM-3D adopting a Lagrangian incremental formulation. Interaction between the workpiece and grain in dry contact conditions was simulated considering a constant Coulomb friction coefficient of 0.2 [24]. Since grain hardness (2085 Vickers microhardness) is much higher than workpiece hardness (62 HRC), the former was modeled as a rigid body with real grain geometry acquired by computed tomography. The workpiece was represented as a deformable prismatic body with dimensions sufficient to achieve the minimum stroke required to reach complete grain penetration defined by the chosen cut depth. The workpiece was modeled with tetrahedral elements distributed within windows characterized by decreasing element dimensions near the interaction zone. Specifically, four mesh windows were prepared: three on the workpiece body with element sizes of 1 mm, 0.5 mm and 0.1 mm, respectively, and a mesh window following grain movement with an element size of 0.03 mm. In this way, the smallest

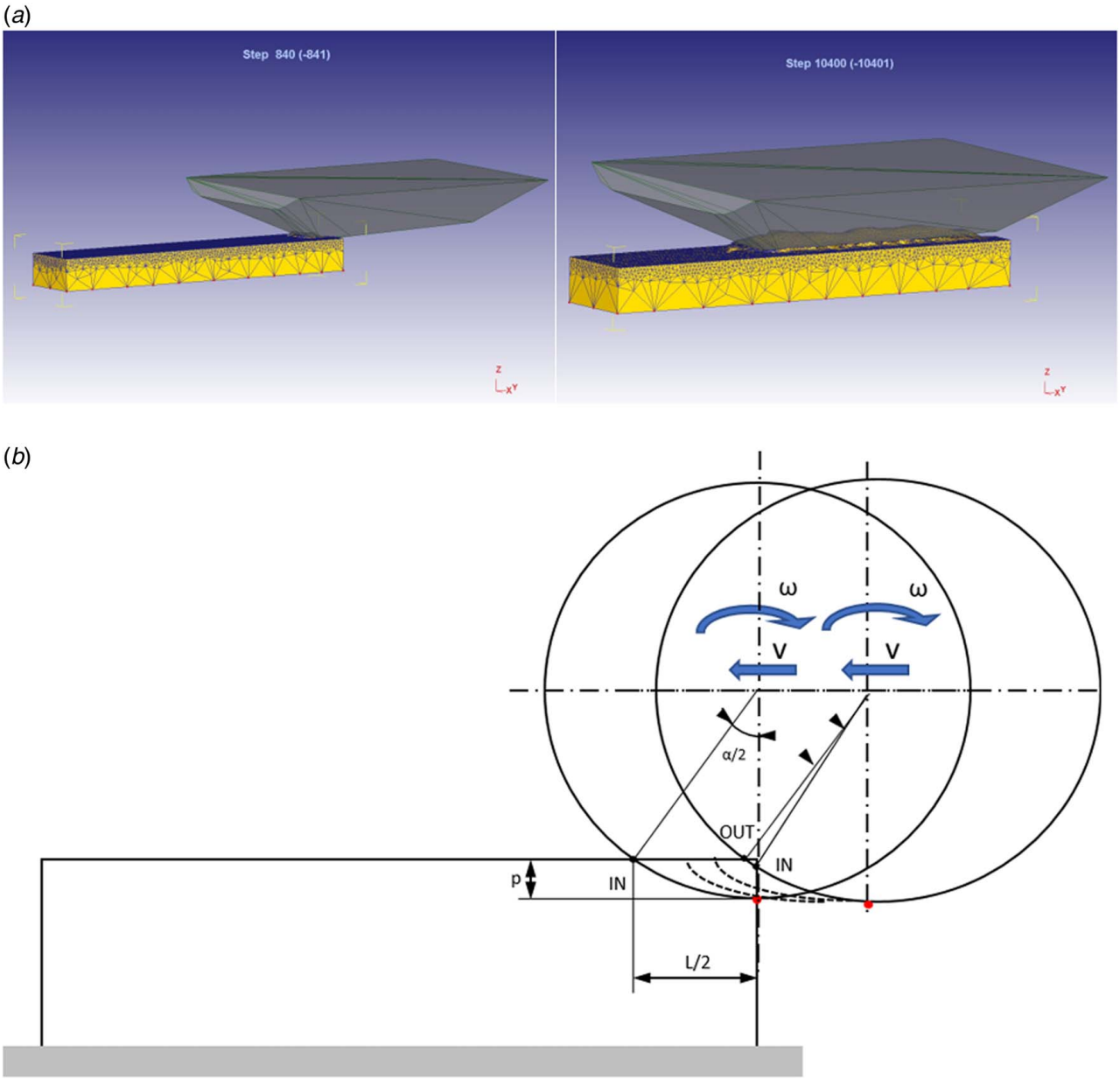

Fig. 2 (*a*) Single grain grinding model mesh and (*b*) kinematics

element was equal to one-third of the cut depth. The total number of workpiece elements and nodes was 16,975 and 3867, respectively. The workpiece mesh was set as an absolute mesh, while the grain mesh was set as a relative mesh with a size ratio of 20 (Fig. 2(*a*)). Translation and rotational movements were assigned to the grain to represent the real kinematics during experiments. Up-grinding was considered, with the grain trajectory programmed such that the center of rotation was located above the workpiece edge. The virtual grinding wheel had a diameter of 152 mm and interacted with the workpiece as shown in Fig. 2. Zero velocity boundary conditions were applied to the lower workpiece surface to maintain its position fixed in the space (grey zone in Fig. 2(*b*)).

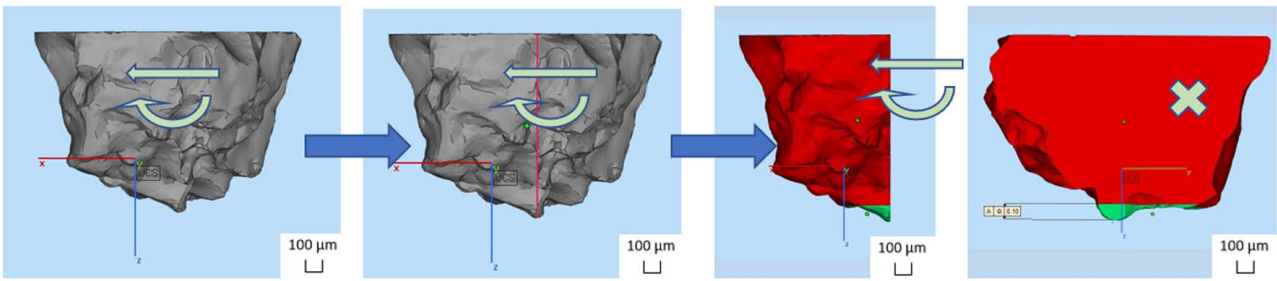

Fig. 3 Grain contact area measurement

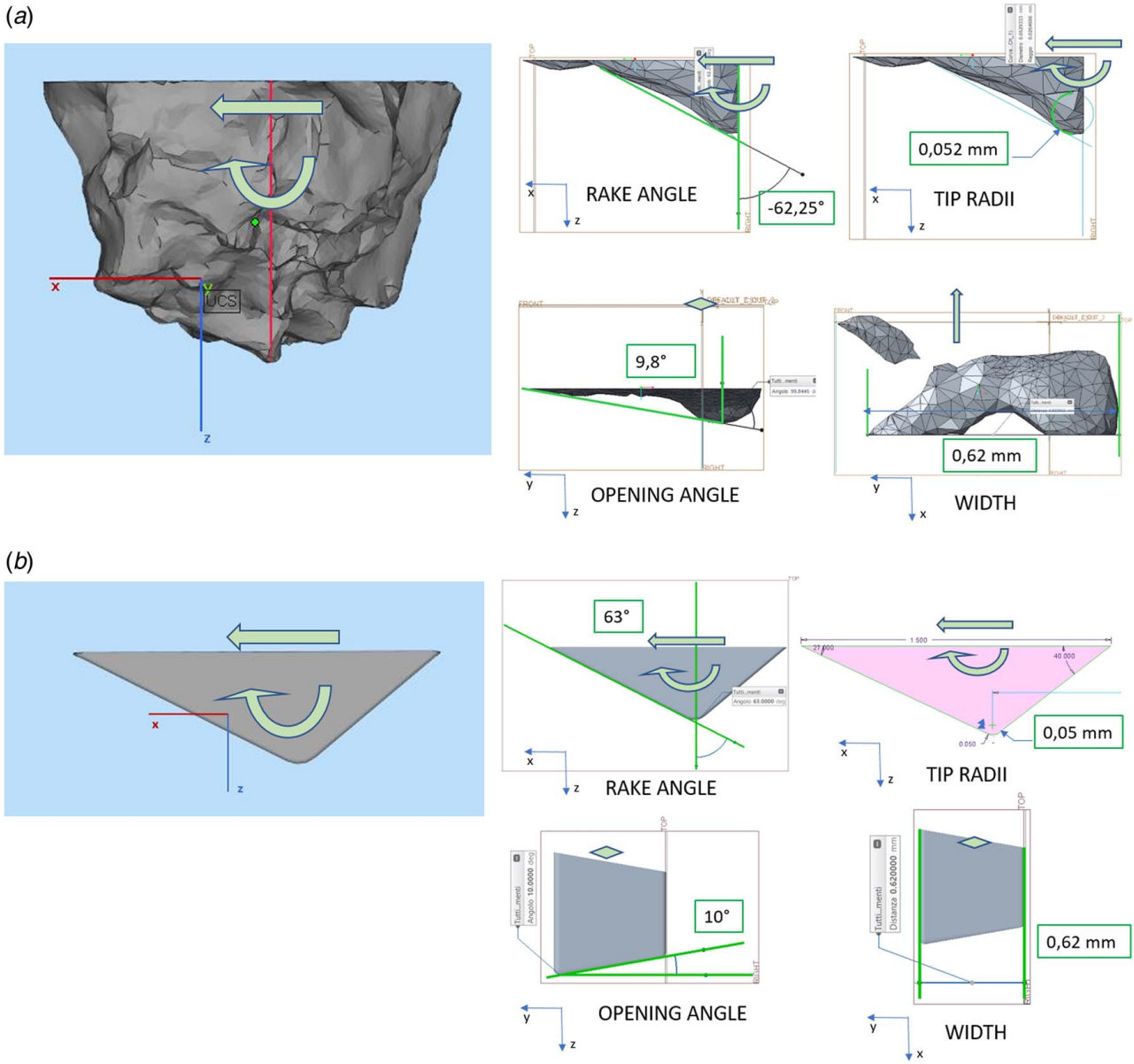

Fig. 4 Grain geometry analysis: (*a*) real grain and (*b*) defined grain

Variable time steps were applied to reduce calculation time, with the grain-workpiece interaction phase assigned a time step of 100 ns and the remaining rotation phase 100 μs. Due to the high degree of detail required to represent the problem in a FEM environment, many difficulties were faced due to limited computing power, especially employing real grain geometry characterized by a large number of elements.

Grain Geometry Analysis. The first simulation approach was implemented using real grain geometry acquired by computed tomography to gather as much information as possible in relation to the real contact area. Subsequently, a grain with defined geometry was implemented with characteristics comparable with that of the real grain, including a negative rake angle of 62 deg, fillet radius of 0.05 mm, opening angle of 9.8 deg, a width of 0.6 mm and the same nominal contact area. The contact area was considered as the projected chip load area on the Y-Z plane and measured with STL editor software Magics Materialize, as shown in Fig. 3. The arrows represent the translational and rotational movement of the grain during the simulation and experiments. The nominal contact area between the grain and workpiece was

Table 1 Discretization of real and defined grain geometries

	Real grain geometry	Defined grain geometry
n° nodes	10,292	70
n° elements	46,043	186

Table 2 J&C parameters and material properties of reference material

J&C parameters	A	B	n	T_r	T_m	C	m
Ref. material	2480	1440	0.45	20	1460	0.012	1.1

Material properties	ρ (kg/m^3)	c_p (J/kgK)	λ (W/mK)
Workpiece	7850	354–916	24.57–24.75
Grain	3950	747–1106	6.10–23.71

Table 3 Johnson & Cook coefficient combinations

Runorder	A	B
Ref	2480	1440
r1	1984	1728
r2	1984	1440
r3	1984	1872
r4	2480	1728
r5	1736	1728
r7	1736	1440
r8	1736	1872
r9	2480	1872
r10	1612	1728
r11	1612	1872
r12	1612	1440
r13	1860	1440
r14	1860	1728
r15	1860	1872

measured in correspondence with the cutting depth p by correctly identifying the grain position during experiments. The grain geometry was sectioned along the x-axis in correspondence with the maximum grain height and along the z-axis at a height of p. It can immediately be noted that a very small portion of the grain was actually involved in cutting, for which it was considered plausible to define an equivalent grain geometry and simplify the load simulation phase.

The real and simplified grain, together with their principal geometric characteristics, are compared in Fig. 4.

The main differences between the grains with real and defined geometry related to the number of elements and nodes required to represent the body. In particular, the grain with defined geometry could be discretized with dozens of nodes and elements, while the real geometry required tens of thousands of nodes and elements, as reported in Table 1.

The real grain geometry, despite representing the contact area very accurately, required a large quantity of data for detailed representation and needs weeks for calculation. The equivalent defined grain geometry required much less data for simulation, allowing single grit grinding forces to be extensively examined by introducing a good estimate of cutting loads with a lower calculation time of some days.

Material Flow Stress Curve Optimization. Fused aluminum oxide was assigned as the grain material. For the workpiece material the Johnson-Cook model, widely used to represent materials viscoplastic hardening and thermal softening with high strain-rate dependency [25,26], was employed to describe material flow according to Eq. (1).

$$\sigma = (A + B \cdot \varepsilon^n) \cdot (1 + C \cdot \ln\frac{\dot{\varepsilon}}{\dot{\varepsilon}_o}) \cdot [1 - \left(\frac{T - T_r}{T_m - T_r}\right)^m] \quad (1)$$

where the parameter A is the initial yield strength of the material at room temperature, $\dot{\varepsilon}$ is the equivalent plastic strain rate normalized with a reference strain-rate $\dot{\varepsilon}$ e, T_r is the room temperature, T_m is the melting temperature of the material, and B, C, n and m are model parameters. The parameters n, m and C are the strain-hardening exponents, thermal softening exponent and strain-rate sensitivity, respectively. An initial reference material [27] with the same surface hardness (62 HRC) of case-hardened gear [28] was considered. The authors have determined its J&C coefficients through a characterization method based on split Hopkinson pressure bar (SHPB) technology, which leads to characterize the reference material properties at high strain rates and high temperatures. Having the same hardness as case-hardened steel but diverse carbon content, differences in material behaviour were accounted, therefore, an optimization strategy based on the procedure proposed in Ref. [29] to calibrate the J&C material coefficients was introduced.

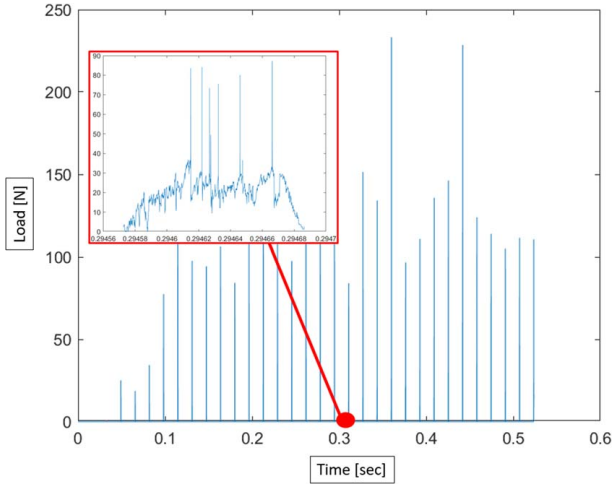

Fig. 5 Example of macroscopic and microscopic (enlarged frame) effective stress peaks (#2.1)

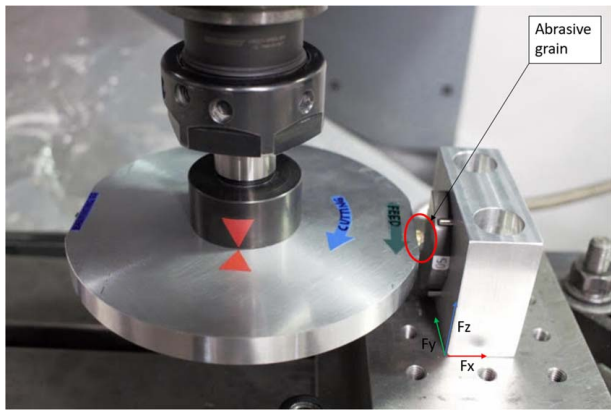

Fig. 6 Experimental setup

As A and B were the parameters of greatest influence on the flow stress curve, these constants were varied over a range of values and FEM simulations were employed to find the most suitable combination, which was subsequently used to simulate the single-grit grinding process. Coefficient A was varied over five levels from the reference value of 2480 MPa to −20%, −25%, −30% and −35% of this value. Coefficient B was instead varied over three levels from the reference value of 1440 MPa to +20% and +30% of this value. Flow stress coefficients and material properties of the reference material are reported in Table 2.

The J&C coefficient combinations proposed for the flow stress optimization plan are shown in Table 3. The Cockroft-Latham model was used to predict the fracture criterion for chip formation with the material critical value set to 0.22 [27].

Simulation Data Analysis. DEFORM-3D output data were processed in Matlab to remove abnormal peaks and extract the correct values of loads for each rotation. All full grain rotations corresponded to a macroscopic peak in the load curve, while each macroscopic peak was composed of a number of micro-peaks. The resulting value was taken as the average of all micro-peaks within each macro-peak. A representative example is shown in Fig. 5, where macroscopic peaks can be seen within the main graph, while micro-peaks can be seen on a shorter time-scale within the enlarged frame.

Each micro-peak exhibited typical grain machining behavior comprising rubbing, ploughing and cutting phases. The rubbing

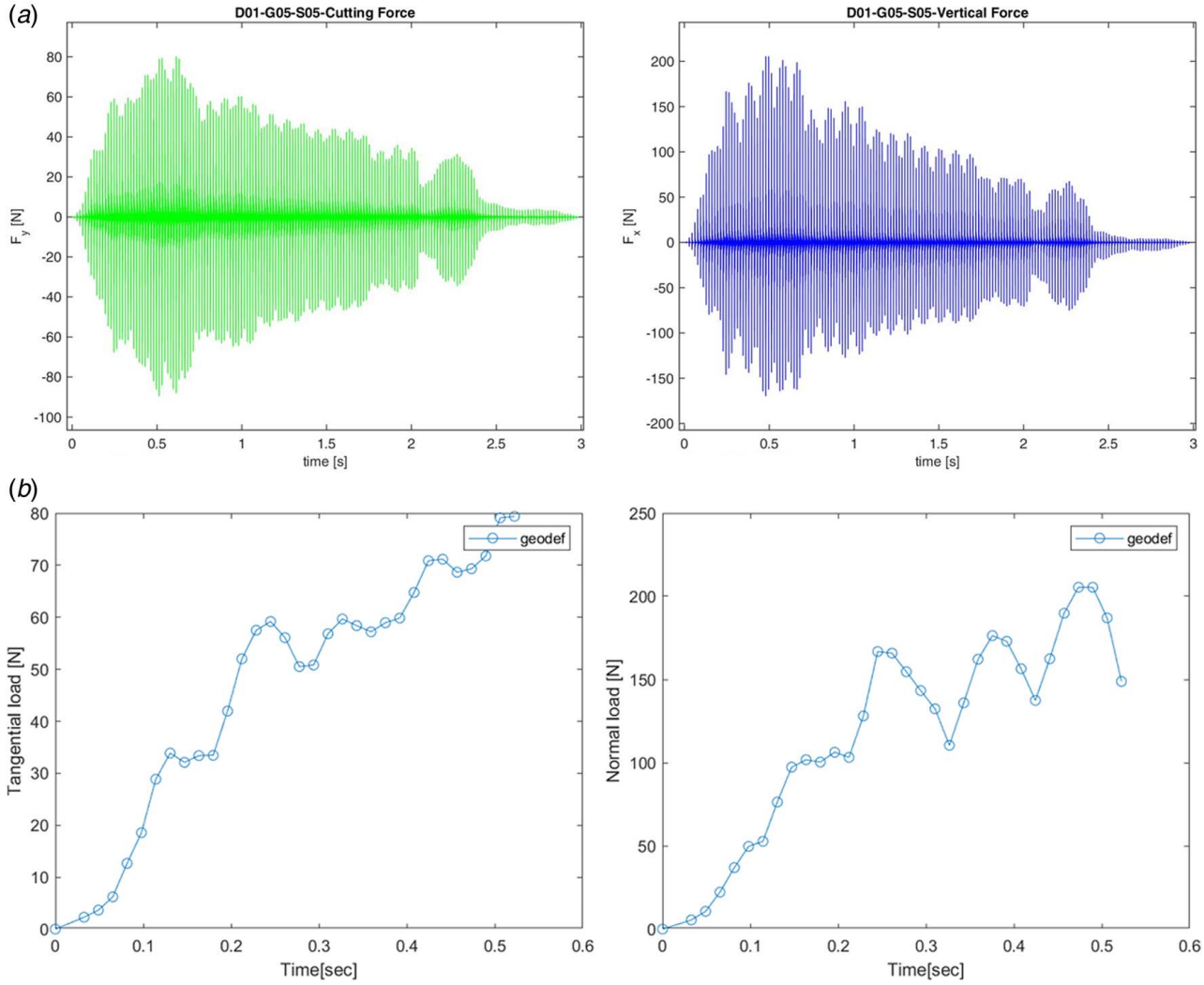

Fig. 7 (*a*) Acquired and (*b*) Fy and Fx force signals used for simulation comparison for single-grain grinding experiments performed with w = 384 rad/s, $v = 8.6$ mm/s, and $p = 0.1$ mm

phase, due to elastic deformation only, is the shortest and generally results in a negligible effect in terms of contributing to material removal. The ploughing phase, involving both elastic and plastic deformation but without chip removal, plays an important role in the surface formation and energy consumption. The cutting phase, where actual chip formation takes place, involves elastic and plastic deformation as well as chip removal. Since ploughing consumes a lot of energy without directly contributing to material removal, this phase is responsible for the specific energy of grinding being much higher than other cutting processes. The highest micro-peaks during the ploughing phase were due to the presence of piled-up material at the edges of incisions left from previous passes that the grain encountered during subsequent rotations. This interaction caused automatic remeshing during the simulation. The maximum value was not representative of the whole pass, for which data processing was required to properly analyze the forces peaks to determine the most representative value of load for each rotation.

Experimental Setup. Experiments were performed on a computer numerical controlled (CNC) milling machine, shown in Fig. 6. A single-grain configuration was employed by attaching a single abrasive grain to a 150 mm diameter metallic holder with epoxy resin. Cutting force components were measured using a Kistler 9257B dynamometer with a frequency acquisition equal to 10,000 Hz performing three repetitions for each test. Pure fused aluminum oxide (Al_2O_3) abrasive grains with a FEPA size of 16 were used for the experiments, while case-hardened 27MnCr5 steel was employed as the workpiece material. Heat treatment was first performed on the workpiece to replicate a tooth gear surface and achieve a hardness of 62 HRC to a depth of at least 1 mm, after which the blocks were pre-ground. Tests and simulations were performed using the process parameters adopted in previous work [30]: $\omega = 384$ rad/s; $v = 8.6$ mm/s; $p = 0.1$ mm. Force signals acquired by the dynamometer were then processed in Matlab to extract the load component for each full rotation of the grinding wheel. A higher than the usual grain dimension and depth of cut for the gear grinding process was used to ease the simulation calculation in that the goal is to validate the single grinding grain model calibrating the flow stress curve and optimizing the grain tool geometry. Equivalent maximum chip thickness which combines depth of cut, feed rate and wheel speed was estimated for each rotation at 30 µm when the grain engaged completely the material, by means:

$$h_{eq} = p \cdot \frac{v}{w}$$

Whereas equivalent chip thickness h_{eq} is the layer removed at wheel speed [30].

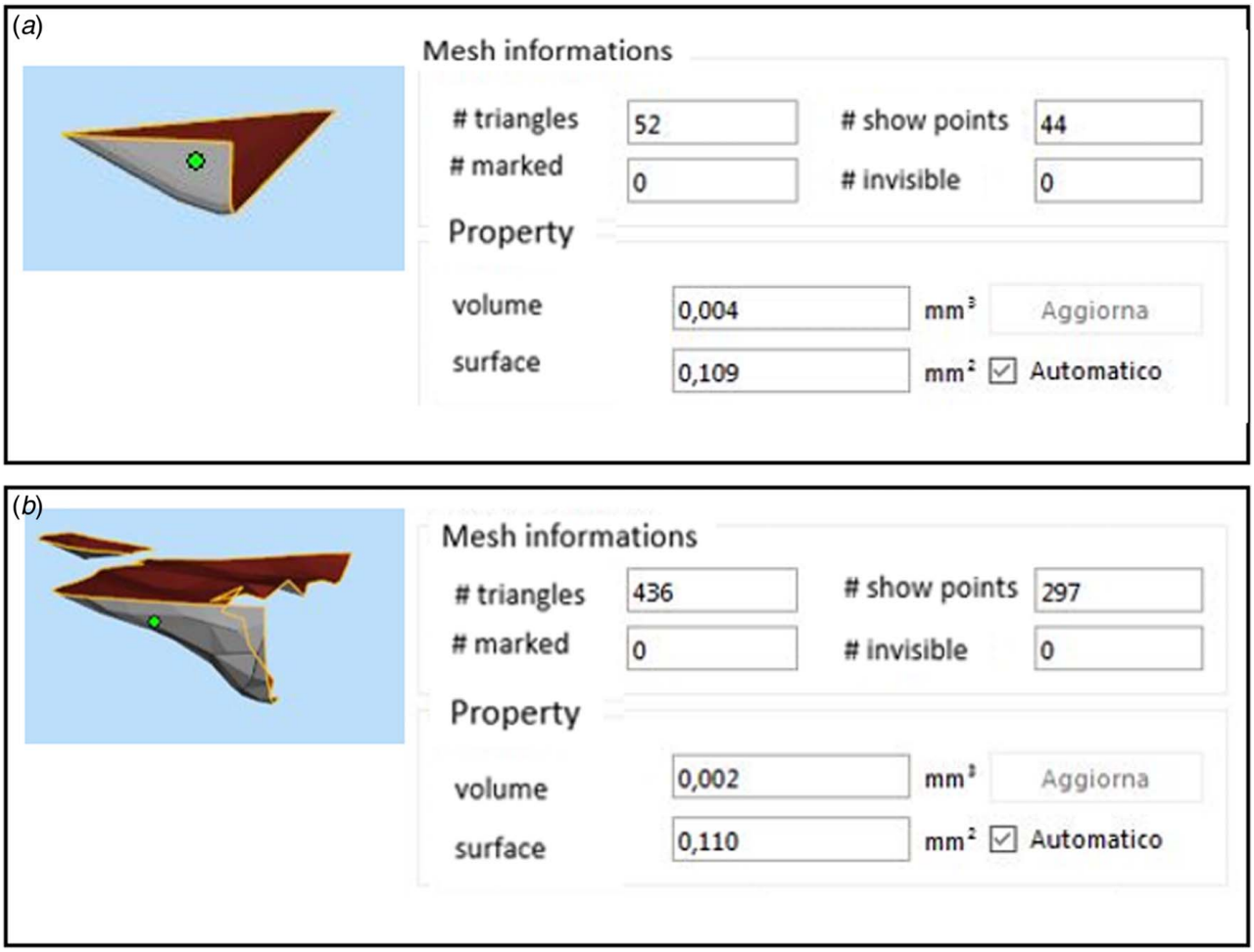

Fig. 8 Nominal contact area measurements: (*a*) defined grain geometry and (*b*) real grain geometry

Results and Discussion

Experimental Results. The main objective of this research activity was to allow accurate prediction of cutting forces during single-grit grinding deriving new flow stress coefficients for the case-hardened depth of 27MnCr5 automotive gear steel. With this in mind, experimental and simulation outcomes were compared through load calculation. Force signals acquired during experiments with a sampling rate of 10,000 Hz are provided in Figs. 7(*a*) and 7(*b*). Fx was typically greater than Fy, while Fz is not reported as it was considered negligible. Experimental grinding forces progressively increased with cutting depth during the initial transient phase. The maximum absolute grinding force was generally achieved once the instantaneous center of rotation of the virtual wheel was located above the workpiece edge and a full cut was achieved, after which forces decreased due to grain wear. For the process parameter set in question, maximum grinding forces and maximum contact area were therefore expected to be achieved after 0.45 s, corresponding to the 27th rotation. Maximum values were in fact achieved shortly after this point due to elastic springback of the material. To check the maximum grinding force value attained for this material and set of process parameters, the minimum required simulation time was therefore 0.5 s from the beginning of the test. Experimental results were taken from a preliminary work [30] and used to check the feasibility of using the equivalent defined grain geometry and the flow stress curve describing case-hardened depth steel.

Comparison Between Real and Defined Grain Simulations. Due to the time-consuming nature of the simulation employing real grain geometry, a faster simulation adopting equivalent defined grain geometry was implemented to compare cutting behavior with the real grain geometry model and verify the calculated forces with experimental data. The nominal contact area was the same for both grain geometries, approximately 0.110 mm^2. In Fig. 8, information regarding the contact surface is reported. Some differences can be observed in relation to the number of elements and nodes generated by the STL editor software. The real grain geometry contact surface was discretized with 436 elements and 297 nodes, while the defined equivalent grain geometry contact surface was reduced to 52 elements and 44 nodes.

Tangential and normal loads were analyzed to verify whether the cutting behavior of the workpiece was comparable while adopting different grain geometries with the same process parameters. This was confirmed to be the case, with an average percentage difference of 10% up to a processing time of 0.114 s, as shown in Fig. 9. As the grain was modeled as a rigid body with the same portion of material remaining in contact during each rotation, it was, therefore, possible to hypothesize that the trends observed with the defined grain were also achieved with real grain geometry. The equivalent defined grain geometry was therefore considered as representing a valid alternative to the real grain geometry.

Comparison Between Defined Grain and Experimental Results. Comparison of tangential and normal loads for the simulated defined grain geometry and experimental results is presented in Fig. 10. It can be observed that simulated load values were generally overestimated compared to experimental outcomes. This is possibly due to the fact that a suitable constitutive material model had not yet been implemented. The average percentage difference

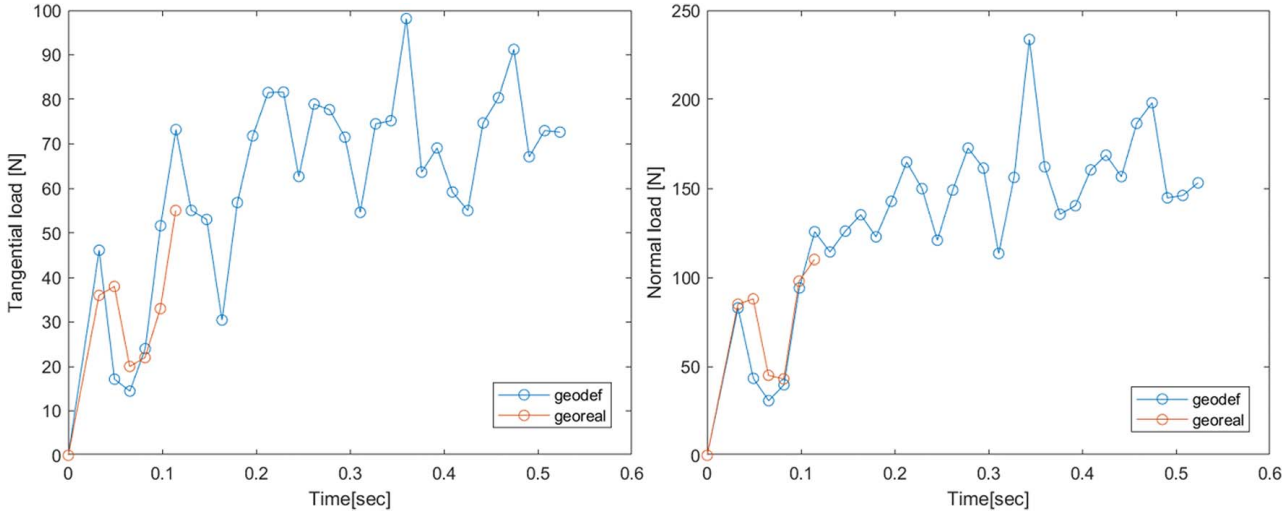

Fig. 9 Simulated tangential and normal load trend comparison between real grain and equivalent defined grain geometry with reference flow stress curve

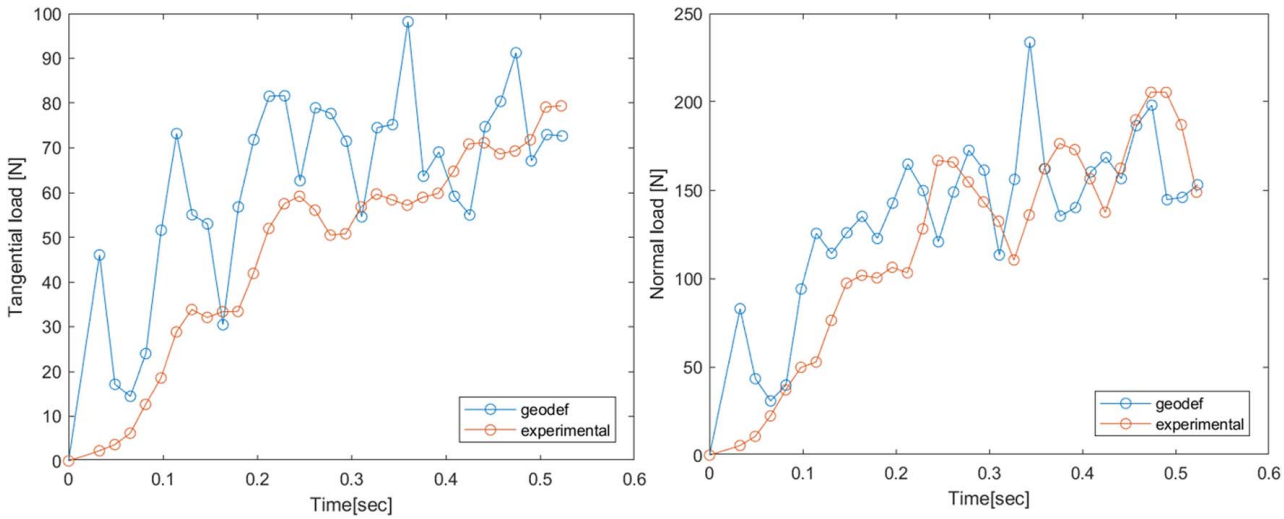

Fig. 10 Comparison of tangential and normal loads for simulated equivalent defined grain geometry and experimental results utilizing reference material flow stress curve

between the calculated defined grain and experimentally determine loads was 25% for tangential forces and 10% for normal forces. Optimization of the flow stress curve was, therefore, necessary to reduce the deviation between simulated and experimental forces.

Flow Stress Optimization. To deal with this challenge, optimization of the flow stress curve through inverse parameter identification was performed. For the initial set of J&C parameters, values of a reference material from the literature were adopted. Based on the simulation adopting equivalent defined grain geometry, a percentage difference between experimental and simulated outcomes of about 25% in tangential loads and 10% in normal loads was obtained. Therefore, the goal of this phase consisted of finding the J&C parameter set that would offset these percentage differences between the calculated load values and experimental data. To this end, a simulation plan consisting of five levels of parameter A and three levels of parameter B was implemented.

Comparison between the reference flow stress and proposed combinations of J&C coefficients was considered in terms of percentage differences between calculated loads with the aim of finding the J&C coefficients achieving a reduction in tangential forces of 25% and normal forces of 10%. Percentage differences between the reference simulation, adopting the flow stress of the reference material, and the different J&C coefficient sets are shown for both tangential and normal loads in Fig. 11. The blue and orange dotted lines represent the percentage difference targets for tangential (25%) and normal (10%) loads, respectively.

The most suitable parameter set was the r2 configuration (Table 3), with values of A equal to 1984 MPa and B equal to 1440 MPa, achieving percentage reductions of 23.84% and 9.85% compared to the values achieved with the reference coefficients for tangential and normal loads, respectively. A final simulation was therefore implemented with the new flow stress coefficient set (A = 1984 MPa; B = 1440 MPa; C = 0.012; n = 0.45; m = 1.1). Good agreement between load values was reached, with average percentage differences of 13% and 3,5% observed for tangential and normal loads, respectively, as shown in Fig. 12.

Model Validation. The same procedure was applied to a second single-grit grinding test (G02) to validate the calibrated flow stress curve. The same process parameters were chosen but with another grain having different geometric characteristics and shape, characterized by a rake angle equal to 53 deg, a tip radius of 0.05 mm,

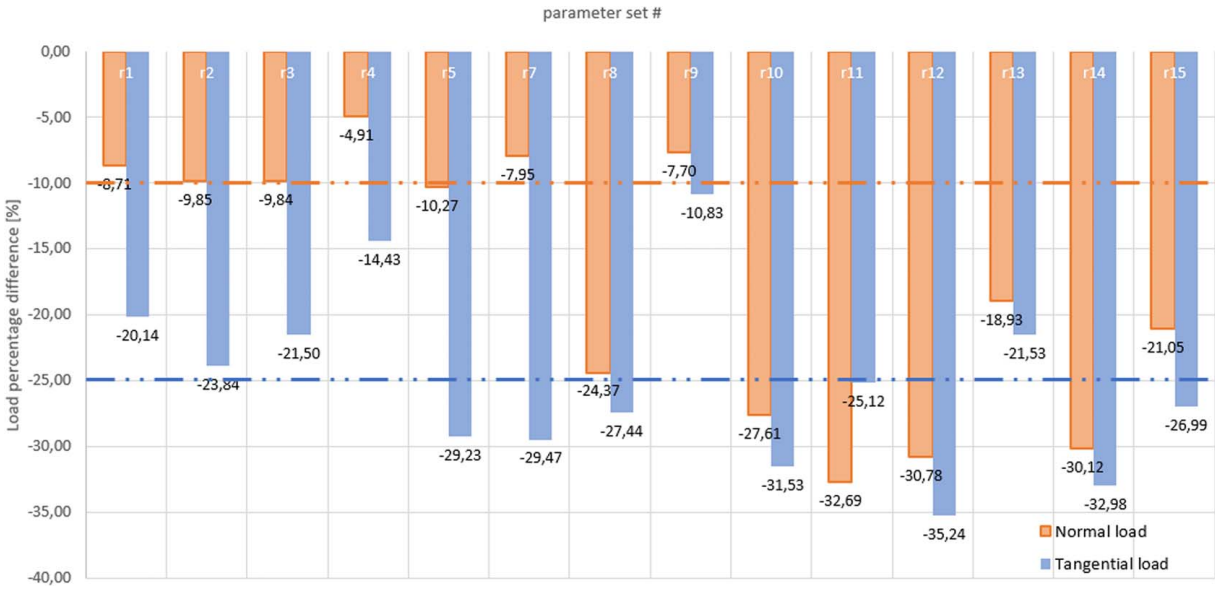

Fig. 11 Percentage difference between reference flow stress curve and DoE J&C coefficient sets for tangential and normal load values

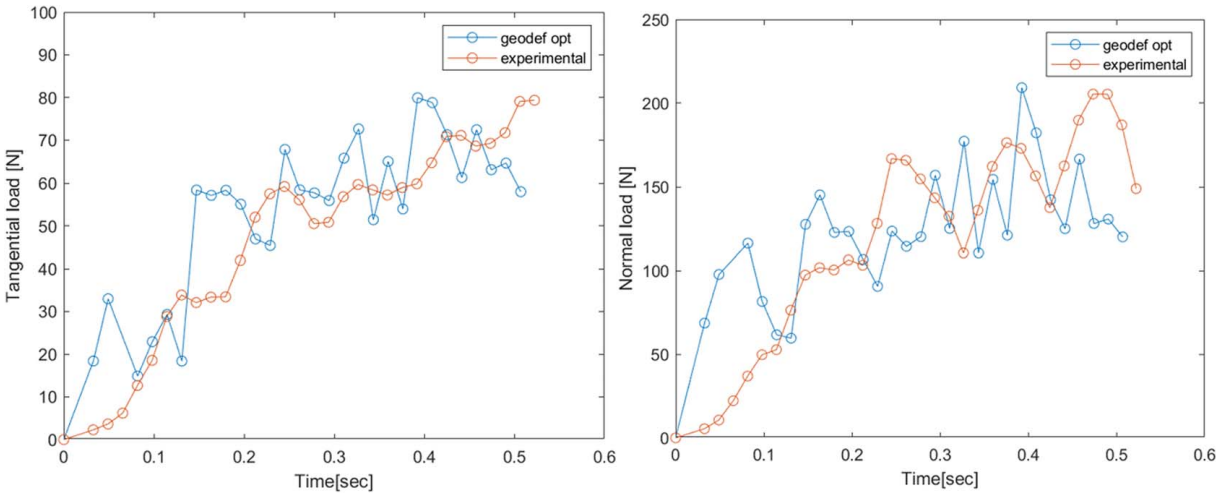

Fig. 12 Tangential and normal load trend comparison between experimental and simulated equivalent defined grain geometry with optimized flow stress curve

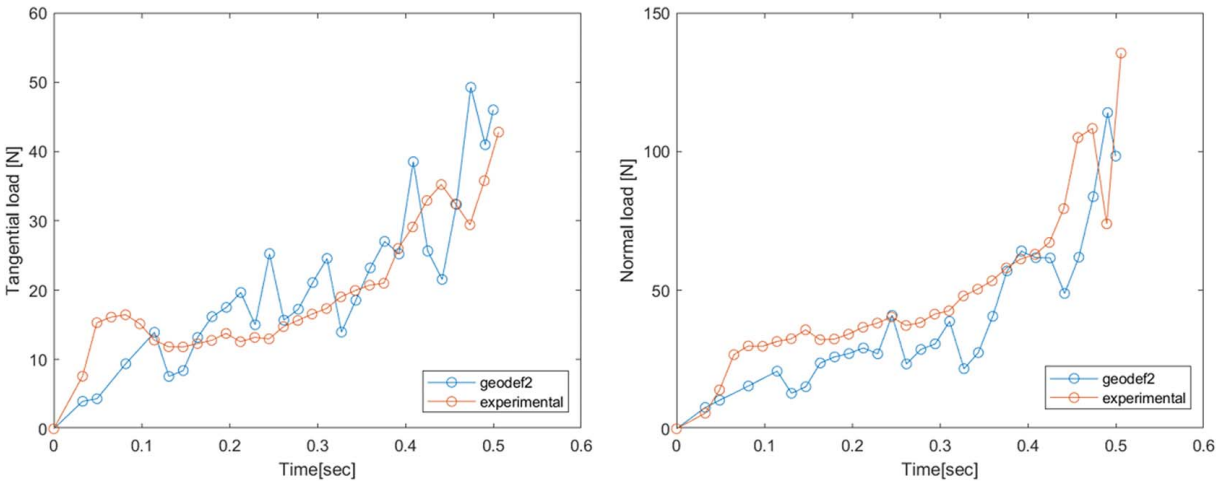

Fig. 13 G02 Tangential and normal load trend comparison between experimental and equivalent defined grain geometry simulation results with optimized flow stress curve

an opening angle of 12 deg and a total width of 0.55 mm with a contact area of 0.211 mm^2. In this case, the grain geometry showed a totally different shape characterized by a double macro-asperity, which denoted a larger contact area despite the reduction of the width grain and shape. After analysis of the real grain geometry, the equivalent defined grain geometry was designed to represent the real contact area between the grain and workpiece. With reference to Fig. 13, it is possible to firstly observe that the use of the same process parameters with grains characterized by slightly different geometry leads to different load behavior. Tangential and normal loads were lower than the first test due to the lower rake angle and width, which implies a reduced ploughing effect. Good agreement between experimental and calculated tangential and normal loads was confirmed achieving a maximum percentage difference of 9% and 12% respectively, thus validating the new flow stress curve.

Conclusion

A single grit grinding FEM simulation has been developed to predict maximum load values based on the real grain geometry implementing a new flow stress curve for 27MnCr5 case-hardened steel and considering the real kinematics of grinding tests. The main results can be summarized as follows:

- As the simulation of real grain geometry was time-consuming, an equivalent defined grain geometry was implemented by considering the same nominal contact area between the grain and workpiece. Good alignment between real and equivalent defined geometry was observed, implying that real grain geometry can be simplified and replaced with defined grain geometry if the equivalent contact area between grain and workpiece is provided.
- An inverse simulation-based method was applied to identify the most suitable Johnson & Cook material coefficients for the hardened depth of the automotive gear case-hardened steel in question, 27MnCr5. Different combinations of J&C coefficients were analyzed with the aim of achieving target reductions in tangential and normal forces. With the most suitable set of flow stress coefficients defined, the single grit grinding process was simulated with the previously defined grain geometry to check the calibration of the material flow stress model. Good agreement was observed between calculated and measured tangential and normal forces with a maximum percentage difference of 13%.

A further test and simulation were implemented adopting the same process parameters to validate the model and new flow stress curve for a different grain geometry, confirming good alignment with the experimental results achieving a maximum percentage difference of 12%. Further works will be focused on thermal defect prediction on gears due to the dry grinding process starting from the single grain action.

Conflict of Interest

There are no conflicts of interest.

Data Availability Statement

The authors attest that all data for this study are included in the paper.

Nomenclature

p = depth of cut
T = temperature
c_p = specific heat
T_m = material melting temperature
T_r = material room temperature
A, B, C, n, m = model constants
ε = strain
$\dot{\varepsilon}$ = strain rate
$\dot{\varepsilon}_o$ = reference strain rate
σ = stress
λ = thermal conductivity
v = feed rate
ρ = density
ω = cutting speed

References

[1] Guerrini, G., Landi, E., Peiffer, K., and Fortunato, A., 2018, "Dry Grinding of Gears for Sustainable Automotive Transmission Production," J. Cleaner Prod., **176**, pp. 76–88.
[2] He, B., Wei, C., Ding, S., and Shi, Z., 2019, "A Survey of Methods for Detecting Metallic Grinding Burn," Meas. J. Int. Meas. Confed., **134**, pp. 426–439.
[3] Brinksmeier, E., Aurich, J. C., Govekar, E., Heinzel, C., Hoffmeister, H.-W., Klocke, F., Peters, J., Rentsch, R., Stephenson, D. J., Uhlmann, E., Weinert, K., and Wittmann, M., 2006, "Advances in Modeling and Simulation of Grinding Processes," CIRP Ann.—Manuf. Technol., **55**(2), pp. 667–696.
[4] Doman, D. A., Warkentin, A., and Bauer, R., 2009, "Finite Element Modeling Approaches in Grinding," Int. J. Mach. Tools Manuf., **49**(2), pp. 109–116.
[5] Mohamed, A. M. O., Warkentin, A., and Bauer, R., 2012, "Variable Heat Flux in Numerical Simulation of Grinding Temperatures," Int. J. Adv. Manuf. Technol., **63**(5–8), pp. 549–554.
[6] Anderson, D., Warkentin, A., and Bauer, R., 2008, "Experimental Validation of Numerical Thermal Models for dry Grinding," J. Mater. Process. Technol., **204**(1–3), pp. 269–278.
[7] Linke, B., Duscha, M., Vu, A. T., and Klocke, F., 2011, "FEM-Based Simulation of Temperature in Speed Stroke Grinding with 3D Transient Moving Heat Sources," Adv. Mater. Res., **223**, pp. 733–742.
[8] Malkin, S., and Guo, C., 2007, "Thermal Analysis of Grinding," CIRP Ann.—Manuf. Technol., **56**(2), pp. 760–782.
[9] Guo, C., and Malkin, S., 2000, "Energy Partition and Cooling During Grinding," J. Manuf. Process., **2**(3), pp. 151–157.
[10] Tönshoff, H. K., Peters, J., Inasaki, I., and Paul, T., 1992, "Modelling and Simulation of Grinding Processes," CIRP Ann., **41**(2), pp. 677–688. ISSN 0007-8506.
[11] Chen, X., and Rowe, W. B., 1996, "Analysis and Simulation of the Grinding Process. Part I: Generation of the Grinding Wheel Surface," Int. J. Mach. Tools Manuf., **36**(8), pp. 871–882.
[12] Chen, X., and Brian Rowe, W., 1996, "Analysis and Simulation of the Grinding Process. Part II: Mechanics of Grinding," Int. J. Mach. Tools Manuf., **36**(8), pp. 883–896.
[13] Chen, X., Rowe, W. B., Mills, B., and Allanson, D. R., 1996, "Analysis and Simulation of the Grinding Process. Part III: Comparison with Experiment," Int. J. Mach. Tools Manuf., **36**(8), pp. 897–906.
[14] Chen, X., Rowe, W. B., Mills, B., and Allanson, D. R., 1998, "Analysis and Simulation of the Grinding Process. Part IV: Effects of Wheel Wear," Int. J. Mach. Tools Manuf., **38**(1–2), pp. 41–49.
[15] Aurich, J. C., Braun, O., Warnecke, G., and Cronjäger, L., 2003, "Development of a Superabrasive Grinding Wheel with Defined Grain Structure Using Kinematic Simulation," CIRP Ann.—Manuf. Technol., **52**(1), pp. 275–280.
[16] Warnecke, G., and Zitt, U., 1998, "Kinematic Simulation for Analyzing and Predicting High-Performance Grinding Processes," CIRP Ann.—Manuf. Technol., **47**(1), pp. 265–270.
[17] Hecker, R. L., Liang, S. Y., Wu, X. J., Xia, P., and Jin, D. G. W., 2007, "Grinding Force and Power Modeling Based on Chip Thickness Analysis," Int. J. Adv. Manuf. Technol., **33**(5–6), pp. 449–459.
[18] Li, H. N., Yu, T. B., Wang, Z. X., Da Zhu, L., and Wang, W. S., 2017, "Detailed Modeling of Cutting Forces in Grinding Process Considering Variable Stages of Grain-Workpiece Micro Interactions," Int. J. Mech. Sci., **126**(May 2016), pp. 319–339.
[19] Dai, J., Ding, W., Zhang, L., Xu, J., and Su, H., 2015, "Understanding the Effects of Grinding Speed and Undeformed Chip Thickness on the Chip Formation in High-Speed Grinding," Int. J. Adv. Manuf. Technol., **81**(5–8), pp. 995–1005.
[20] Badger, J. A., and Torrance, A. A., 2000, "Comparison of two Models to Predict Grinding Forces From Wheel Surface Topography," Int. J. Mach. Tools Manuf., **40**(8), pp. 1099–1120.
[21] Anderson, D., Warkentin, A., and Bauer, R., 2011, "Experimental and Numerical Investigations of Single Abrasive-Grain Cutting," Int. J. Mach. Tools Manuf., **51**(12), pp. 898–910.
[22] Yang, J. G., Zhou, Z. X., Li, B. Z., and Zhu, D. H., 2011, "Study on the Simulation Model and High-Speed Characteristics of Cylindrical Grinding," Adv. Mater. Res., **223**, pp. 826–835.
[23] Chen, X., Opoz, T. T., and Oluwajobi, A., 2017, "Analysis of Grinding Surface Creation by Single-Grit Approach," ASME J. Manuf. Sci. Eng., **139**(12), p. 121007.
[24] Cai, G. Q., Feng, B. F., Jin, T., and Gong, Y. D., 2002, "Study on the Friction Coefficient in Grinding," J. Mater. Process. Technol., **129**(1–3), pp. 25–29.

[25] Barge, M., Hamdi, H., Rech, J., and Bergheau, J. M., 2005, "Numerical Modelling of Orthogonal Cutting: Influence of Numerical Parameters," J. Mater. Process. Technol., **164–165**, pp. 1148–1153.
[26] Arrazola, P. J., Özel, T., Umbrello, D., Davies, M., and Jawahir, I. S., 2013, "Recent Advances in Modelling of Metal Machining Processes," CIRP Ann.—Manuf. Technol., **62**(2), pp. 695–718.
[27] Wang, C., Ding, F., Tang, D., Zheng, L., Li, S., and Xie, Y., 2016, "Modeling and Simulation of the High-Speed Milling of Hardened Steel SKD11 (62 HRC) Based on SHPB Technology," Int. J. Mach. Tools Manuf., **108**, pp. 13–26.
[28] Guerrini, G., Lerra, F., and Fortunato, A., 2019, "The Effect of Radial Infeed on Surface Integrity in dry Generating Gear Grinding for Industrial Production of Automotive Transmission Gears," J. Manuf. Process., **45**, pp. 234–241.
[29] Eisseler, R., Drewle, K., Grötzinger, K. C., and Möhring, H. C., 2018, "Using an Inverse Cutting Simulation-Based Method to Determine the Johnson-Cook Material Constants of Heat-Treated Steel," Procedia CIRP, **77**(Hpc), pp. 26–29.
[30] Guerrini, G., Lutey, A. H. A., Melkote, S. N., Ascari, A., and Fortunato, A., 2019, "Dry Generating Gear Grinding: Hierarchical two-Step Finite Element Model for Process Optimization," ASME J. Manuf. Sci. Eng., **141**(6), p. 061005.